

MOF-Modified NaCrO₂ Cathode for High-Rate and Wide-Temperature

Applications in Sodium-ion Battery

Yuxi Luo, ‡^a Guojie Chen, ‡^a Zhewen Ma,^{b,*} Xiaoyu Gao,^a Wenguang Zhao,^a Wenxin Tong,^a Yuguang Pu,^a Pinyu Niu,^a Wenqing Yao,^a Hui Fang,^a Maolin Yang,^a Lei Cao,^a Wen Yin,^{c,d} Tingting Yang,^e Mihai Chu,^f Götz Schuck,^g Wenhai Ji,^{c,d,*} Rui Wang,^{h,*} and Yinguo Xiao^{a,*}

^a School of Advanced Materials, Peking University, Shenzhen Graduate School, Shenzhen 518055, China

^b State Key Laboratory of Advanced Processing and Recycling of Nonferrous Metals, School of Materials Science and Engineering, Lanzhou University of Technology, 730050 Lanzhou, China

^c Institute of High Energy Physics, Chinese Academy of Sciences (CAS), Beijing 100049, China

^d Spallation Neutron Source Science Center (SNSSC), Dongguan 523803, China

^e Ernst Ruska-Centre for Microscopy and Spectroscopy with Electrons, Forschungszentrum Jülich GmbH, Jülich 52428, Germany

^f Department of Chemistry, Materials, and Chemical Engineering “Giulio Natta”, Politecnico di Milano, Milano 20133, Italy

^g Department of Structure and Dynamics of Energy Materials, Helmholtz-Zentrum Berlin für Materialien und Energie, Hahn-Meitner-Platz 1, Berlin, 14109, Germany

^h Department of Engineering, University of Cambridge, 17 Charles Babbage Road, Cambridge CB30FS, UK

‡These authors contributed equally to this work.

* Correspondence: Zhewen Ma (marvin90@lut.edu.cn), Wenhai Ji (jiwh@ihep.ac.cn), Rui Wang (rw716@cam.ac.uk), Yinguo Xiao (y.xiao@pku.edu.cn).

Material Synthesis

Sodium carbonate (Na_2CO_3 , Aladdin 99.99%) and chromium trioxide (Cr_2O_3 , Aladdin, 99.99%) are mixed according to the stoichiometric ratio, and the mixture is placed in a ball mill jar for thorough milling to ensure uniform mixing of the reactants and good particle distribution. During the ball milling process, an appropriate amount of grinding media is used, and the milling is conducted at a speed of 300 rpm for 10 hours to avoid particle agglomeration or excessive material wear. The resulting powder mixture after milling should have good uniformity, with minimal large particle residues. After ball milling, the uniformly mixed powder is transferred to a high-temperature furnace for solid-state reaction calcination at an appropriate temperature. The calcination temperature is set at 900°C to ensure complete reaction and the formation of NaCrO_2 . During calcination, the heating rate is controlled at $3^\circ\text{C}/\text{min}$ to avoid thermal shock. The process is maintained for 10 hours under an argon gas atmosphere to ensure complete reaction and crystallization. After calcination, the product is naturally cooled to room temperature.

$\text{Cr}_2(\text{SO}_4)_3 \cdot 6\text{H}_2\text{O}$ (Aladdin, 99.95%) was used as the metal ion source, and trimesic acid (H_3BTC , Aladdin, 98%) was used as the organic ligand during the synthesis process of MOF materials. First, 0.009 mol of $\text{Cr}_2(\text{SO}_4)_3 \cdot 6\text{H}_2\text{O}$ was dissolved in 60 mL of deionized water and stirred thoroughly to prepare the $\text{Cr}_2(\text{SO}_4)_3 \cdot 6\text{H}_2\text{O}$ solution. Simultaneously, H_3BTC corresponding to stoichiometric ratio was dissolved in 120 mL of deionized water. A 0.5 M NaOH solution was then slowly added dropwise to adjust the pH value of the solution to 7, promoting the complete dissolution of H_3BTC and neutralizing the hydrogen ions released. The prepared H_3BTC solution (120 mL) was stirred at 1000 rpm, into which the Cr^{3+} solution was slowly added. After a few minutes, green precipitates (Cr-MOF) gradually appeared in the beaker. The mixture was stirred continuously for 10 hours to ensure the complete formation of the MOF. The synthesized precipitates were then washed multiple times with excess deionized water to remove any residual reactants. The washed precipitates were dried under vacuum at 60°C for 8 hours, followed by further drying at 100°C for 24 hours to remove external moisture. solvents from the MOF. Finally, the dried Cr-MOF samples were stored in a glove box for subsequent characterization and testing. Cr-MOF and the previously synthesized NCO were manually ground using a mortar and pestle, followed by re-calcination at 750°C for 5 hours in Ar to obtain the corresponding $\text{NCO}@t\text{Cr}_2\text{O}_3\text{-C}$ ($t=0.05, 0.10, 0.15$ and 0.20).

Structural characterization

Sample morphologies were analyzed using a ZEISS Supra 55 scanning electron microscope (SEM) and a JEOL-3200FS field-emission transmission electron microscope (TEM) operating at

300 kV, equipped with Energy Dispersive Spectroscopy (EDS) for element distribution analysis. To investigate the crystal structure, X-ray powder diffraction (XRD) and neutron powder diffraction (NPD) patterns were collected. XRD measurements were performed on a Bruker D8 ADVANCE diffractometer with a Cu K α source ($\lambda = 1.5406 \text{ \AA}$) for both pristine powder characterization and *in situ* experiments. NPD experiments were conducted on the Multi-Physics Instrument (MPI) at the China Spallation Neutron Source (CSNS) in Dongguan, China, with each pattern collected for 1 hour to ensure high data quality. Rietveld refinements of XRD and NPD data were carried out using the FullProf Suite program. X-ray photoelectron spectroscopy (XPS) analysis was performed using a focused Al K α monochromatic X-ray source (ESCA Lab220I-XL) to determine the valence states of Cr, with the C 1s peak at 284.8 eV used for calibration. The hard XAS experiment was performed with the assistance of Götz Schuck (Hard XAS Scientist at KMC2, Berlin, Germany), from the Department of Structure and Dynamics of Energy Materials, Helmholtz-Zentrum Berlin für Materialien und Energie, Hahn-Meitner-Platz 1, Berlin, 14109, Germany. Cr L-edge soft X-ray absorption spectroscopy (sXAS) Measurements were carried out at the GELEM Dipole beamline at the BESSY II electron storage ring operated by the Helmholtz-Zentrum Berlin für Materialien und Energie. The total electron yield (TEY) mode was measured at 300 K under an ultra-high vacuum (UHV) condition of 10^{-9} Torr. Electrochemical performance was evaluated using CR2032 button cells.

Electrochemical characterization

Cathode electrodes were prepared by dissolving 80 wt% cathode material, 10 wt% acetylene black, and 10 wt% PVDF in N-methyl-2-pyrrolidone (NMP). The resulting slurry was uniformly coated onto aluminum foils and dried in a vacuum oven at 100 °C for 6 hours. The electrolyte is a solution of 1 M NaClO₄ in propylene carbonate ethylene carbonate dimethyl carbonate (PC/EC/DMC=1:1:1 volume ratio) and fluorinated ethylene carbonate (2% volume ratio). Half-cells were assembled in an argon-filled glove box using sodium metal foil as the anode. Galvanostatic charge-discharge tests were performed over a voltage range of 2.0-3.6 V at different rates (1 C = 120 mA g⁻¹) using a Neware battery cycler. Cyclic voltammetry (CV) and electrochemical impedance spectroscopy (EIS) were performed using a CHI660E electrochemical workstation. *In situ* EIS charge-discharge processes were controlled using an Ivium electrochemical workstation. In the full cell, the cathode (NCO@Cr₂O₃-C) had an areal loading of approximately 1-1.2 mg cm⁻², and the N/P ratio is 1.1.

GITT is used to calculate the diffusion coefficient D based on Fick's law, and its basic formula is:

$$D_{Na^+} = \frac{4}{\pi\tau} \left(\frac{mV_m}{MA} \right)^2 \left(\frac{\Delta E_s}{\Delta E_\tau} \right)^2$$

A represents the contact surface area between the electrode and the electrolyte, τ is the duration of the current pulse. The voltage change during the current pulse is denoted by ΔE_τ , while the steady-state voltage change after the pulse is denoted by ΔE_s . V_m is the molar volume.

The key formula in variable speed CV is used to describe the relationship between peak current and scan rate, usually based on the Randles Sevcik equation. For reversible systems, the relationship between peak current and scan rate is as follows:

$$i_p = (2.69 \times 10^5) \cdot n^{3/2} \cdot A \cdot D^{1/2} \cdot C \cdot v^{1/2}$$

Among them: i_p is peak current (A); n is the number of electrons transferred in an electrochemical reaction; A is the effective surface area of the electrode (cm^2); D is the diffusion coefficient of the active substance in the electrolyte (cm^2/s); C is the concentration of active substances in the electrolyte (mol/cm^3); v is the scanning rate (V/s).

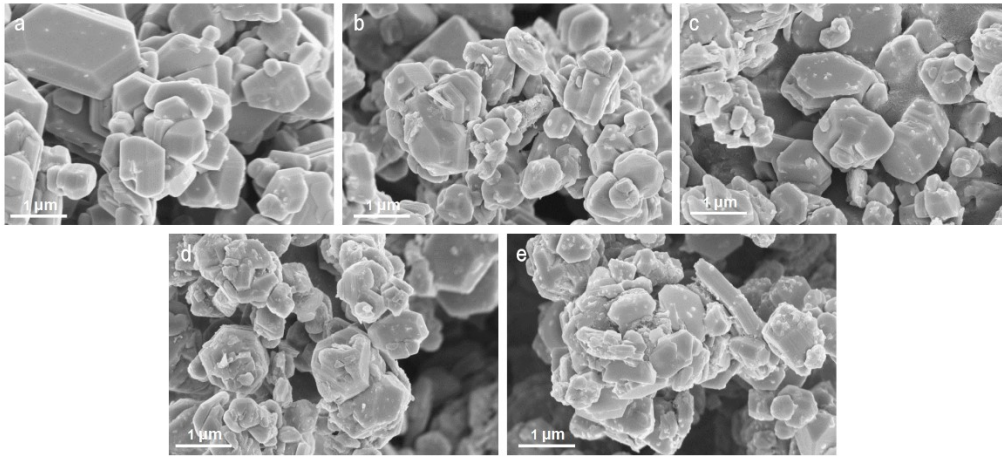


Figure S1. The SEM images of (a) NCO, (b) NCO@0.05Cr₂O₃-C, (c) NCO@0.10Cr₂O₃-C, (d) NCO@Cr₂O₃-C and (e) NCO@0.20Cr₂O₃-C.

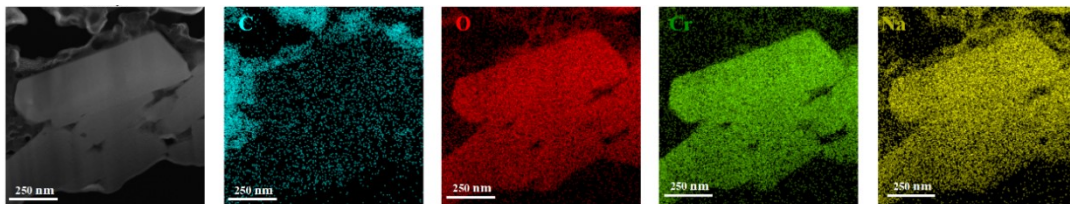


Figure S2. EDS elemental mapping of NCO grain.

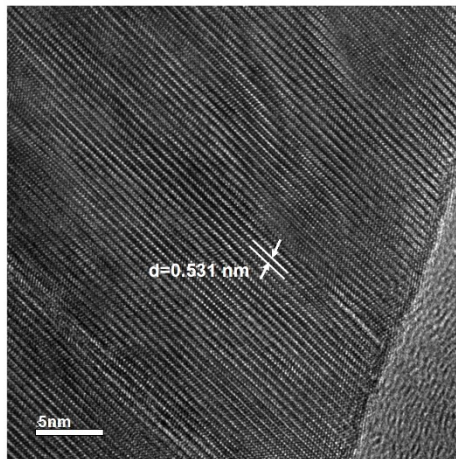


Figure S3. TEM image of NCO along the [003] zone axis.

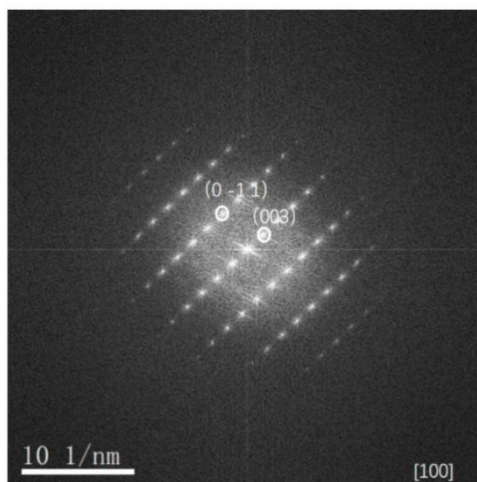


Figure S4. SAED patterns viewed along the [100] zone axis of NCO.

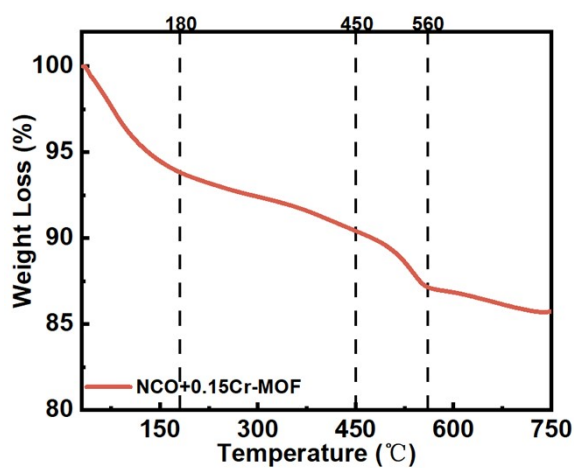


Figure S5. The TGA diagram of NCO+0.15Cr-MOF.

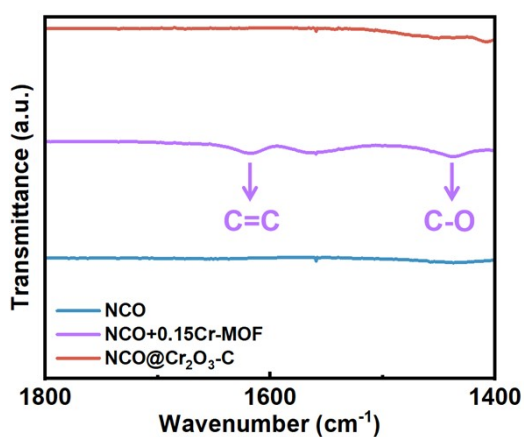


Figure S6. The infrared spectroscopy (IR) data diagram of NCO, NCO+0.15Cr-MOF and NCO@Cr₂O₃-C.

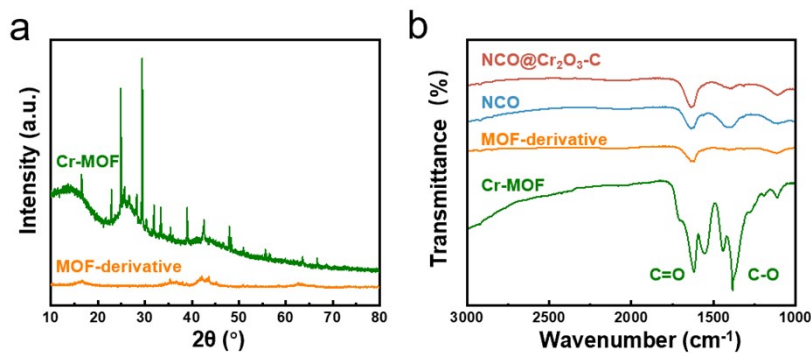


Figure S7. (a) XRD patterns of Cr-MOF and MOF-derivative. (b) FTIR data of Cr-MOF, MOF-derivative, NCO and NCO@Cr₂O₃-C.

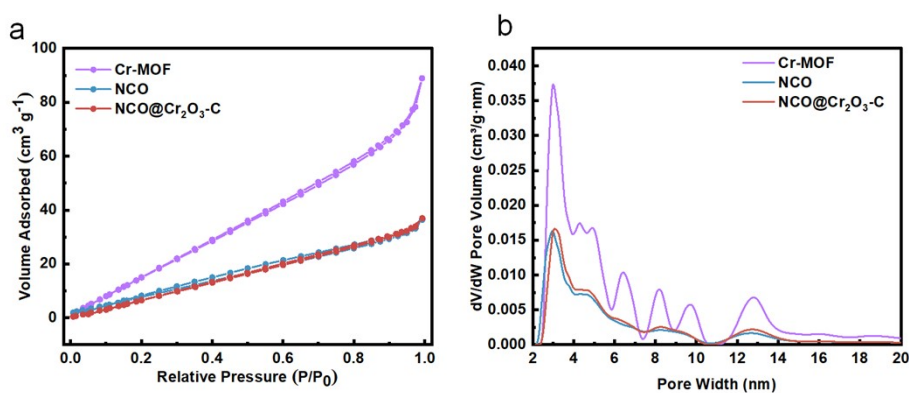


Figure S8. (a) Nitrogen adsorption-desorption isotherms and (b) pore size distribution curves for Cr-MOF, NCO, and NCO@Cr₂O₃-C.

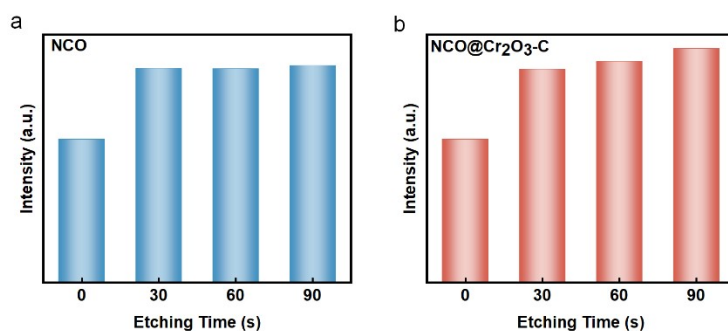


Figure S9. (a) The area ratio for the Cr³⁺ peak of the XPS results at different etching depths of the NCO. (b) The area ratio for the Cr³⁺ peak of the XPS results at different etching depths NCO@Cr₂O₃-C.

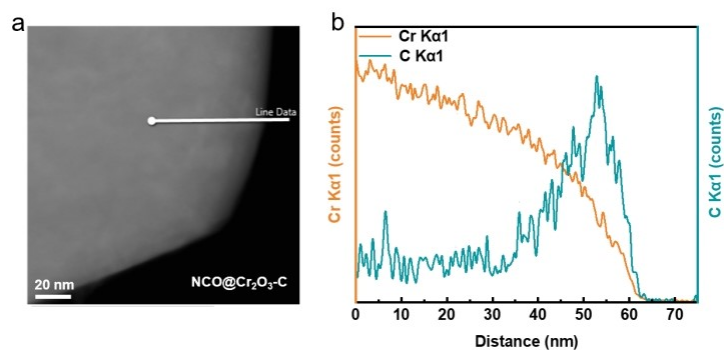


Figure S10. (a) TEM image of NCO@Cr₂O₃-C. (b) EDS Line Scan Results of NCO@Cr₂O₃-C.

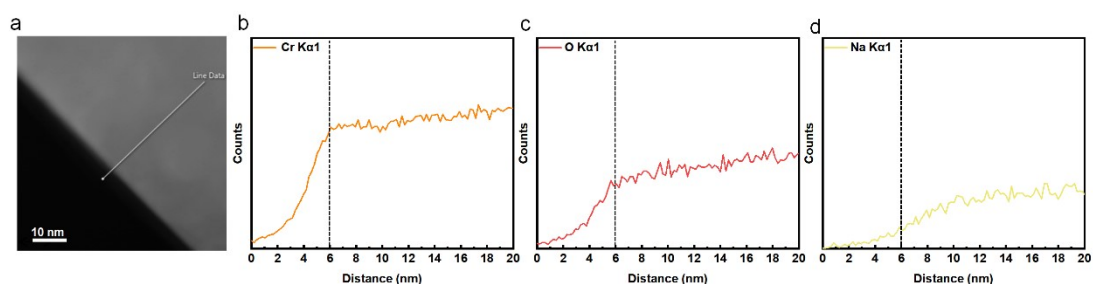


Figure S11. (a) TEM image of NCO@Cr₂O₃-C. (b) EDS Line Scan Results of Cr K α 1 NCO@Cr₂O₃-C. (c) EDS Line Scan Results of O K α 1 NCO@Cr₂O₃-C. (d) EDS Line Scan Results of Na K α 1 NCO@Cr₂O₃-C.

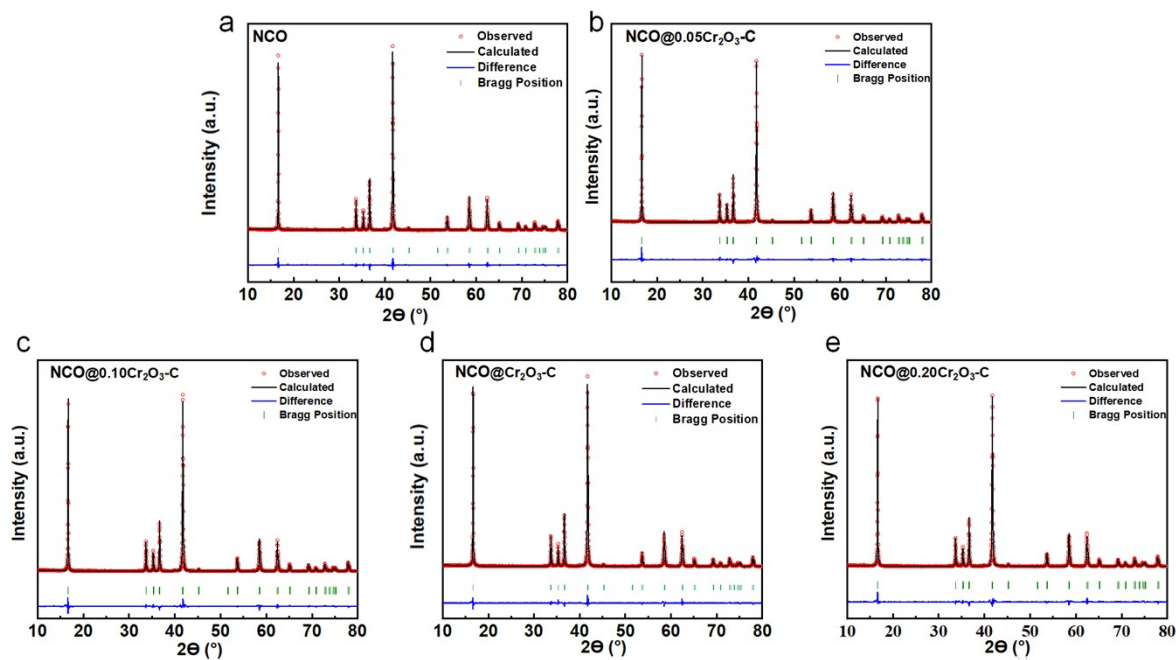


Figure S12. The XRD refinement pattern for samples.

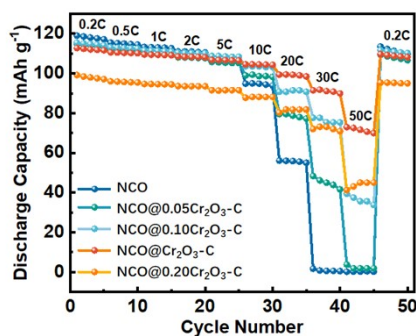


Figure S13. The rate performance comparison of NCO, NCO@0.05Cr₂O₃-C, NCO@0.10 Cr₂O₃-C, NCO@ Cr₂O₃-C and NCO@0.20 Cr₂O₃-C at different rates.

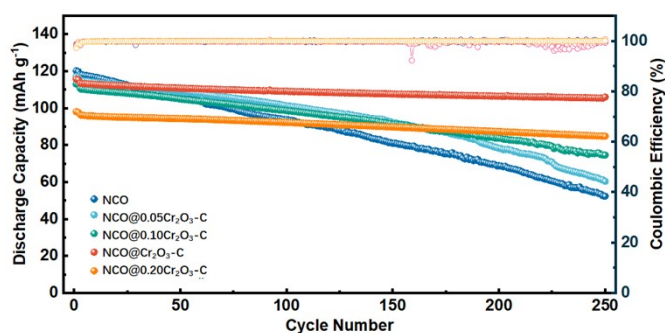


Figure S14. Long-term cycling retention of NCO, NCO, NCO@0.05Cr₂O₃-C, NCO@0.10 Cr₂O₃-C, NCO@ Cr₂O₃-C and NCO@0.20 Cr₂O₃-C at rates of 3.33C (1C=120mA·g⁻¹).

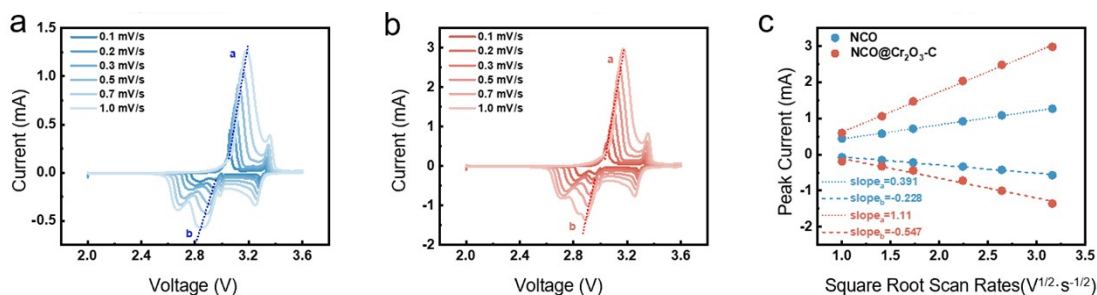


Figure S15. (a) Variable scan rate CV curves from 0.1 to 1 mV s⁻¹ of NCO. (b) Variable scan rate CV curves from 0.1 to 1 mV s⁻¹ of NCO@Cr₂O₃-C. (c) The results of linear fitting for the absolute value of peak current intensity ($|I_p|$) plotted against the square root of the scan rate ($v^{1/2}$) for NCO and NCO@Cr₂O₃-C.

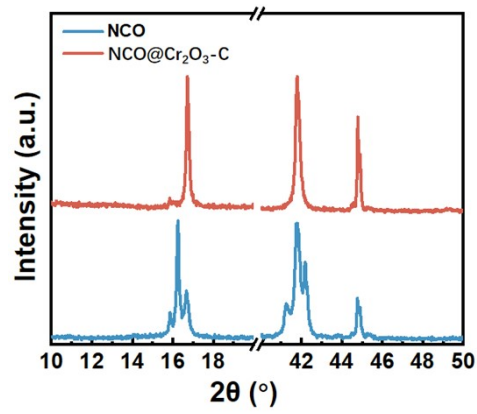


Figure S16. The XRD data of NCO and NCO@Cr₂O₃-C after long cycles.

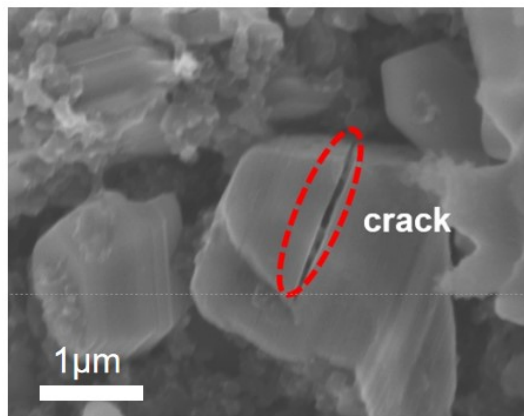


Figure S17. The SEM images of NCO grains after long cycles.

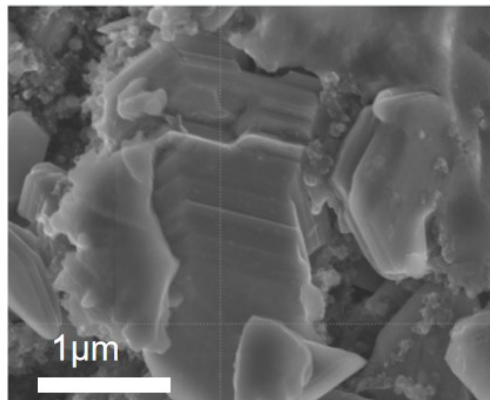


Figure S18. The SEM images of NCO@Cr₂O₃-C grains after long cycles.

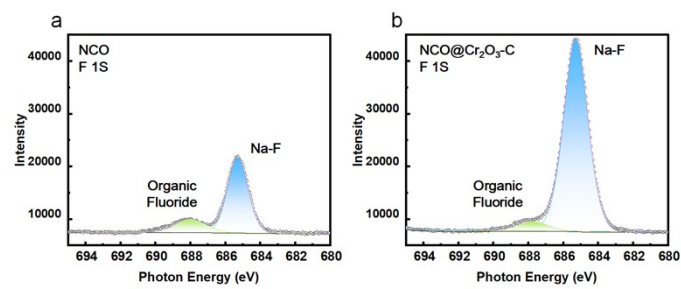


Figure S19. Comparative F 1s XPS spectra of cycled NCO and NCO@Cr₂O₃-C electrodes.

Table S1. The porosity data from the BET of NCO, Cr-MOF and NCO@Cr₂O₃-C

	BET Surface Area (m ² /g)	Average Particle Size (nm)	Pore volume (cm ³ /g)
Cr-MOF	111.6051	53.7610	0.088235
NCO	47.9428	125.1492	0.040047
NCO@Cr ₂ O ₃ -C	58.4858	102.5891	0.040819

Table S2. Refine parameter list of XRD data of NCO, NCO@0.05Cr₂O₃-C, NCO@0.10Cr₂O₃-C, NCO@Cr₂O₃-C and NCO@0.20Cr₂O₃-C

	Lattice parameters			Chi2
	a-axis/ Å	c-axis/ Å	Rwp/%	
NCO	2.9742(3)	15.9585(1)	13.3	2.64
NCO@0.05Cr ₂ O ₃ -C	2.9736(2)	15.9563(2)	11.6	2.35
NCO@0.10Cr ₂ O ₃ -C	2.9736(4)	15.9572(1)	11.0	2.07
NCO@Cr ₂ O ₃ -C	2.9734(2)	15.9561(2)	11.2	2.12
NCO@0.20Cr ₂ O ₃ -C	2.9734(3)	15.9582(2)	12.2	2.44

Table S3. Refine parameter list of NPD data of NCO and NCO@Cr₂O₃-C

	Lattice parameters			Chi2
	a-axis/ Å	c-axis/ Å	Rwp/%	
NCO	2.9746(3)	15.9655(2)	3.12	11.4
NCO@Cr ₂ O ₃ -C	2.9747(4)	15.9663(3)	4.30	9.17

Table S4. The performance comparison with similar studies

Compound	First Q (mAh/g)	Final Q (mAh/g), no of cycle	Decay rate (mAh/g cycle)	Remarks	Ref
NaCrO ₂	120@4.0C	100,50	-0.400		1
C-coated NaCrO ₂	116@0.042C	110,40	-0.150		2
	121@0.167C	109,300	-0.040		3
	116.3@0.83C	85.7,500	-0.061		4
	123.6@1.0C	110,40	-0.340		5
Cr ₂ O ₃ -coated NaCrO ₂	117.7@1.0C	98.6,300	-0.064		6
Na _{0.97} Cr _{0.97} Ti _{0.03} O ₂	124@0.2C	116.6,100	-0.074	Ti-doped	7
Na _{0.94} Cr _{0.97} Nb _{0.03} O ₂	106.6@5.0C	113,35	-0.171	Nb-doped	8
This work	115.7@3.33C	106.2,250	-0.038		

References

1. S. Komaba, C. Takei, T. Nakayama, A. Ogata and N. Yabuuchi, *Electrochemistry Communications*, 2010, **12**, 355-358.
2. J.-J. Ding, Y.-N. Zhou, Q. Sun and Z.-W. Fu, *Electrochemistry Communications*, 2012, **22**, 85-88.
3. C.-Y. Yu, J.-S. Park, H.-G. Jung, K.-Y. Chung, D. Aurbach, Y.-K. Sun and S.-T. Myung, *Energy & Environmental Science*, 2015, **8**, 2019-2026.
4. S. M. Kang, M.-S. Kim, Y. Jeoun, C. Hudaya and Y.-E. Sung, *Bulletin of the Korean Chemical Society*, 2019, **40**, 857-862.
5. A. Bhardwaj and A. K. Panwar, *Applied Surface Science*, 2022, **573**.
6. S. Wang, F. Chen, T.-y. Zhu, X.-d. He, J.-y. Liao, L.-m. Zhang, X. Ding, Q. Hu and C.-h. Chen, *Acs Applied Materials & Interfaces*, 2020, **12**, 44671-44678.
7. Y. Shao, Z.-f. Tang, J.-y. Liao and C.-h. Chen, *Chinese Journal of Chemical Physics*, 2018, **31**, 673-676.
8. S. Wang, F. Chen, H.-y. He, Y.-r. Zhu, H.-b. Liu and C.-h. Chen, *Journal of Alloys and Compounds*, 2022, **925**.